

# Surface $r$ -modes and burst oscillations of neutron stars

Umin Lee

Astronomical Institute, Tohoku University, Sendai, Miyagi 980-8578, Japan  
lee@astr.tohoku.ac.jp

## ABSTRACT

We study the  $r$ -modes propagating in steadily mass accreting, nuclear burning, and geometrically thin envelopes on the surface of rotating neutron stars. For the modal analysis, we construct the envelope models which are fully radiative or have a convective region. We simply call the former radiative models and the latter convective models in this paper. As the angular rotation frequency  $\Omega$  is increased, the oscillation frequency  $\omega$  of the  $r$ -modes in the thin envelopes deviates appreciably from the asymptotic frequency  $\omega = 2m\Omega/l'(l' + 1)$  defined in the limit of  $\Omega \rightarrow 0$ , where  $\omega$  is the frequency observed in the corotating frame of the star, and  $m$  and  $l'$  are the indices of the spherical harmonic function  $Y_{l'}^m$  representing the angular dependence of the modes. We find that the amplitudes of the fundamental  $r$ -modes with no radial nodes of the eigenfunctions are strongly confined to the equatorial region, and  $\omega$  becomes only weakly dependent on  $\Omega$ , gathering in a frequency range of  $\omega/2\pi \lesssim 10\text{Hz}$ , at rapid rotation rates. We also find that the fundamental  $r$ -modes in the convective models are destabilized by strong nuclear burning in the convective region. Because of excessive heating by nuclear burning, the corotating-frame oscillation frequency  $\omega$  of the  $r$ -modes in the convective models becomes larger, and hence the inertial-frame oscillation frequency  $|\sigma|$  becomes smaller, than those of the corresponding  $r$ -modes in the radiative models, where  $\sigma = \omega - m\Omega$  is negative for the  $r$ -modes of positive  $m$ . We find that the relative frequency change  $f = -(\sigma_{conv} - \sigma_{rad})/\sigma_{rad}$  is always positive and becomes less than  $\sim 0.01$  for the fundamental  $r$ -modes of  $l' > |m| + 1$  at  $|\sigma_{rad}|/2\pi \sim 300\text{Hz}$  for  $m = 1$  or at  $|\sigma_{rad}|/2\pi \sim 600\text{Hz}$  for  $m = 2$ , and that we need to consider the  $r$ -modes of  $l'$  much larger than  $|m|$  for values of  $f$  as small as  $\sim 0.001$ , where  $\sigma_{conv}$  and  $\sigma_{rad}$  denote the oscillation frequencies for the convective and the radiative envelope models, respectively.

*Subject headings:* instabilities — stars: neutron — stars: oscillations — stars : rotation

## 1. Introduction

X-ray flux fluctuations observed in type I X-ray bursts in LMXB's (see, e.g., Strohmayer et al 1996, 1997 for so called burst oscillations) are quasi-periodic oscillations whose frequencies are found in a frequency range around  $\sim 300\text{Hz}$  or around  $\sim 600\text{Hz}$ . During a burst, from the onset to the tail, the oscillation frequency in a given source usually increases with time by a small amount and gets saturated to an asymptotic frequency in the tail. The observed frequency drifts are generally less than  $\sim 1\%$  of the mean frequency (e.g., Cumming & Bildsten 2000). However, the time evolution of burst oscillations are not always that simple. In fact, some X-ray burst sources have been reported to show a temporal decrease of the oscillation frequency in the tail of bursts (e.g., Strohmayer 1999, Miller 2000, Munro et al. 2000), or to show simultaneously two oscillation frequencies separated by a few Hz in a burst (Miller 2000, Galloway

et al 2001, Munro et al 2002). Burst oscillations could be very important for neutron star physics. On the assumption that the oscillation frequencies are directly tied to the spin frequency of the star, the stability of the asymptotic frequency found in the tail of bursts separated by a few years has been used to determine some of the physical parameters of binary systems (e.g., Strohmayer et al 1998, Gilles et al 2002). For recent observational and theoretical developments concerning burst oscillations as well as thermonuclear bursts on neutron stars, see a review paper by Strohmayer & Bildsten (2003).

As a model for burst oscillations, Strohmayer et al (1997) proposed that the oscillations are produced by inhomogeneous hot burning spots, the burning fronts of which are expanding laterally on the surface of a rotating neutron star, and that the frequency drifts are associated with the vertical expansion and contraction of the burning spots conserving angular momentum. The model was later refined by Cumming & Bildsten (2000), and Cumming et al (2001) concluded that the possible amount of relative frequency changes expected in the model was by a factor of 2 to 3 smaller than the largest observed values (see also Munro, Özel, & Chakrabarty 2002). This model also has a difficulty in explaining the persistence of the oscillations to the tail of a burst, in which no inhomogeneity to produce the oscillations will remain because all the surface area has been reached by the burning fronts. Spitkovsky, Levin, & Ushomirsky (2002), on the other hand, discussed the global hydrodynamical flow in the ocean of an accreting neutron star, by taking into account the rapid rotation and the lift-up of the burning ocean, and conjectured that Jupiter-type vortices created in strong zonal fluid currents driven in a nuclear burst are responsible for burst oscillations in the tail.

It was Heyl (2001) who suggested that the burst oscillations could be produced by the  $r$ -modes of low azimuthal wavenumber  $m = 1$  or  $m = 2$  traveling in the surface ocean of the neutron star. The  $r$ -modes are retrograde toroidal modes and are called Rossby waves in geophysical context (see, e.g., Greenspan 1968, Pedlosky 1987). The  $r$ -modes in mass-accreting envelopes on the surface of a *slowly* rotating neutron star have been discussed by Strohmayer & Lee (1996), who found that the fundamental  $r$ -modes with no radial nodes of the eigenfunctions are all pulsationally stable except for the cases of mass-accretion rates  $\dot{M}$  as low as  $\dot{M}/\dot{M}_{Edd} \sim 0.001$ , where  $\dot{M}_{Edd}$  denotes the Eddington rate. In this paper, we extend the previous analysis to the cases of rapidly rotating neutron stars, considering that the spin frequencies  $\Omega$  of many neutron stars in LMXB's are now believed to be in a rather narrow range around  $\Omega/2\pi \sim 300\text{Hz}$ . The main points behind the  $r$ -mode model for burst oscillations may be described as follows. Let us assume that strong nuclear burning in the convective phase of a nuclear burst excites surface  $r$ -modes whose time and azimuthal dependence is given by  $\exp(i[\omega_{conv}t + m\phi])$ , where  $\omega$  denotes the oscillation frequency in the corotating frame and the integer  $m$  is the azimuthal wave number. For the  $r$ -modes,  $\omega$  is proportional to and is much smaller than the spin frequency  $\Omega$  of the star, and  $\omega$  is positive for positive  $m$  in the convention we use in this paper. Observers measure the inertial frame frequency  $\sigma_{conv} \equiv \omega_{conv} - m\Omega$ , the magnitude of which is  $|\sigma_{conv}| = m\Omega - \omega_{conv}$ . At the end of the burst, the ocean cools and becomes radiative, and the rotating frame oscillation frequency decreases to  $\omega_{rad}$  and the magnitude of the inertial frame frequency increases to  $|\sigma_{rad}| = m\Omega - \omega_{rad}$ . This model then predicts a fractional increase in the measured inertial frame frequency from the start of the burst to the asymptotic end, which may be given by  $f = -(\sigma_{conv} - \sigma_{rad})/\sigma_{rad}$ . To estimate possible magnitudes of the quantity  $f$ , we calculate in this paper the  $r$ -modes for radiative envelopes and convective envelopes, assuming that the envelopes are in steady state. §2 and 3 briefly describe method of calculation employed in this paper, and §4 is for numerical results, and §5 and 6 are for discussion and conclusion.

## 2. Envelope Calculation

Method of calculation for steadily mass-accreting, nuclear-burning, thin surface envelopes is almost the same as that given in Strohmayer & Lee (1996). No effects of general relativity are included in this paper. If we use the independent variable defined as

$$z = M - M_r, \quad (1)$$

where  $M$  and  $M_r$  are the total mass of the star and the mass contained in the sphere of radius  $r$ , the basic ordinary differential equations for mass-accreting and nuclear-burning thin envelopes in steady state are

$$\frac{dr}{dz} = -\frac{1}{4\pi r^2 \rho}, \quad (2)$$

$$\frac{dp}{dz} = \frac{GM_r}{4\pi r^4}, \quad (3)$$

$$\frac{dL_r}{dz} = -\epsilon_N + \epsilon_\nu + \dot{M} \left( \frac{dU}{dz} - \frac{p}{\rho^2} \frac{d\rho}{dz} \right), \quad (4)$$

and the energy transfer equation in convection zones is

$$\frac{dT}{dz} = \frac{GM_r}{4\pi r^4} \frac{T}{p} \left( \frac{\partial \ln T}{\partial \ln p} \right)_{ad} \equiv \frac{GM_r}{4\pi r^4} \frac{T}{p} \nabla_{ad}, \quad (5)$$

and that in radiative zones is

$$\frac{dT}{dz} = \frac{3\kappa L_r}{64\pi^2 a c r^4 T^3}, \quad (6)$$

where  $\rho$  is the mass density,  $p$  is the pressure,  $T$  is the temperature,  $U$  is the internal energy per gram,  $\kappa$  is the opacity,  $\epsilon_N$  is the nuclear energy generation rate per gram,  $\epsilon_\nu$  is the neutrino energy loss rate per gram,  $L_r$  is the luminosity at  $r$ ,  $\dot{M} = -4\pi r^2 \rho v_r$  is the mass accretion rate, and  $G$ ,  $a$ , and  $c$  are the gravitational constant, the radiation constant, and the velocity of light, respectively. The structure of the chemical composition,  $X_i$ , in steady state is governed by

$$\frac{dX_j}{dz} = \frac{m_j}{\rho \dot{M}} \sum_i n_{ji} r_i, \quad (7)$$

where  $m_j$  is the mass of the particle  $j$ ,  $r_i$  is the rate of the reaction  $i$ , and  $n_{ji}$  is the number of particles  $j$  created ( $n_{ji} > 0$ ) or destroyed ( $n_{ji} < 0$ ) in a reaction  $i$ . The equation of state  $p = p(\rho, T, X_j)$  is that of a perfect gas with radiation, and is given by  $p = p_I + p_e + p_r$ , where  $p_I = n_I k_B T$  with  $n_I$  and  $k_B$  being the number density of ions and the Boltzmann constant,  $p_e$  is the electron gas pressure, and  $p_r = aT^4/3$  is the radiation pressure. The electron gas can be arbitrarily degenerate and relativistic. For hydrogen burning energy generation rates, we use the formulae given in Reeves (1965). The reaction rates of the CNO cycle in high temperature environment are limited by the  $\beta$ -decays of  $^{14}\text{O}$  and  $^{15}\text{O}$ , leading to the saturation of the rates to  $\epsilon_{CNO}^{max} = 5.9 \times 10^{15} Z_{CNO}$  (e.g., Wallace & Woosley 1981), where  $Z_{CNO} = {}^{12}\text{C} + {}^{14}\text{N} + {}^{16}\text{O}$ . For helium burning we include the  $3\alpha$  and  $^{12}\text{C}(\alpha, \gamma)^{16}\text{O}$  reactions, the rates of which are given in Fowler, Caughlan, & Zimmerman (1975). The rate of the carbon burning  $^{12}\text{C} + {}^{12}\text{C}$  reaction is from Patterson, Winkler, & Zaidins (1969), and Arnett & Truran (1969). We apply both weak and strong electron screening corrections to the nuclear energy generation rates following Salpeter & Van Horn (1969). For the energy loss rate due to neutrino emission we employ formulae given by Beaudet, Petrosian, & Salpeter (1967). For opacity, we use a subroutine written by Paczyński (1970) who adopted Cox & Stewart (1970) radiative opacity and the conductive opacity by Hubbard & Lampe (1969) and Canuto (1970).

For given  $M$ ,  $R$ , and  $\dot{M}$ , we integrate the set of differential equations from the surface  $z = 0$  to the bottom  $z = z_b$  of the envelope. At the surface of the envelope, where we assume  $r = R$  and  $M_r = M$ , the surface temperature  $T_s$  and pressure  $p_s$  for a surface luminosity  $L_s$  are given by

$$T_s = (L_s/4\pi R^2 \sigma_{SB})^{1/4}, \quad (8)$$

and

$$p_s = g_s/\kappa(\rho_s, T_s, X_i), \quad (9)$$

where  $g_s = GM/R^2$ , and  $\sigma_{SB} = ac/4$  is the Stefan-Boltzmann constant. The surface luminosity  $L_s$  is determined so that the inner boundary condition  $L_r = 0$  is satisfied at  $z = z_b$ . The envelope models calculated in this way are fully radiative with no convective regions, and are simply called radiative models in this paper.

As discussed by Hanawa & Sugimoto (1982), there develops a convective zone in the nuclear burning region of the surface envelope immediately after the onset of a nuclear flash. To obtain a *convective* model in a nuclear flash, we first in the radiative models determine the location of the base of a convection zone as the inner most layer at which the condition for unstable helium burning

$$\frac{\partial \epsilon_{3\alpha}}{\partial \ln T} \geq 2\epsilon_{CNO}^{max} \left[ 1 - \frac{1}{4} \left( \frac{\partial \ln \kappa}{\partial \ln T} \right)_\rho \right] \quad (10)$$

is satisfied (Cumming & Bildsten 2000), where  $\epsilon_{3\alpha}$  denotes the  $3\alpha$  energy generation rate. We treat the mass extent  $z_c - z_e$  of the convection zone above the base as a parameter, where  $z_c$  and  $z_e$  are the mass depths at the base and at the top of the convection zone, respectively. The temperature gradient in the convection zone is given by equation (5), and the composition is determined by  $\bar{X}_i = \int_{z_e}^{z_c} dz X_i(z)/(z_c - z_e)$ , where  $X_i$  in the integrand is the composition in the corresponding radiative model. When we integrate the basic equations from the surface to the bottom of the envelope so that  $L_r = 0$  at  $z = z_b$ , there appears a strong density discontinuity due to the discontinuous change of compositions  $X_j$  at the boundaries between the convection zone and the radiative regions, at which we assume the continuity of the pressure and the temperature. The envelope models thus constructed to have a convective zone are simply called convective models in this paper.

### 3. Oscillation Calculation

For nonadiabatic and nonradial oscillations of rotating stars, we use the method of solution given by Lee & Saio (1987, 1993). Throughout this paper, we apply the Cowling approximation, neglecting the Euler perturbation of the gravitational potential,  $\Psi'$ . Since separation of variables is not possible for global oscillations of rotating stars, the perturbations are expanded in terms of spherical harmonic functions  $Y_l^m(\theta, \phi)$  for a given  $m$ , assuming axisymmetric equilibrium of the stars. The displacement vector  $\xi(r, \theta, \phi, t)$  is then given by

$$\xi_r = r \sum_{l \geq |m|}^{\infty} S_l(r) Y_l^m e^{i\sigma t}, \quad (11)$$

$$\xi_\theta = r \sum_{l, l' \geq |m|}^{\infty} \left( H_l(r) \frac{\partial}{\partial \theta} Y_l^m + T_{l'}(r) \frac{1}{\sin \theta} \frac{\partial}{\partial \phi} Y_{l'}^m \right) e^{i\sigma t}, \quad (12)$$

$$\xi_\phi = r \sum_{l, l' \geq |m|}^{\infty} \left( H_l(r) \frac{1}{\sin \theta} \frac{\partial}{\partial \phi} Y_l^m - T_{l'}(r) \frac{\partial}{\partial \theta} Y_{l'}^m \right) e^{i\sigma t}, \quad (13)$$

and the Euler perturbation of the pressure,  $p'(r, \theta, \phi, t)$ , for example, is given by

$$p' = \sum_{l \geq |m|}^{\infty} p'_l(r) Y_l^m e^{i\sigma t}, \quad (14)$$

where  $\sigma$  is the oscillation frequency in an inertial frame, and  $l = |m| + 2(j - 1)$  and  $l' = l + 1$  for even modes, and  $l = |m| + 2(j - 1) + 1$  and  $l' = l - 1$  for odd modes where  $j = 1, 2, 3, \dots$ . The expansions of perturbations are substituted into a set of linearized basic equations to give a set of simultaneous linear ordinary differential equations for the expansion coefficients  $S_l(r)$ ,  $H_l(r)$ ,  $iT_{l'}(r)$ ,  $p'_l(r)$ , and so on. In a convective region, the total energy flux  $\mathbf{F}$  is given as the sum of the radiative flux  $\mathbf{F}_{rad}$  and the convective flux  $\mathbf{F}_{conv}$  so that  $\mathbf{F} = \mathbf{F}_{rad} + \mathbf{F}_{conv}$ . Since there exists no reliable theory for the interaction between pulsations and convective motion, for nonadiabatic calculations we assume for simplicity  $\delta(\nabla \cdot \mathbf{F}_{conv}) = 0$  and  $L_{rad} = L_r$  in the convective zone, where  $L_r = 4\pi r^2 F_r$  and  $L_{rad} = 4\pi r^2 F_{rad,r}$ .

The inner mechanical boundary condition we employ is given by  $p' = 0$  (McDermott & Taam 1987), and the inner thermal boundary condition is  $|\delta s / c_p| \ll 1$  (see, Lee & Baraffe 1995), where  $s$  is the specific entropy, and  $c_p$  is the specific heat at constant pressure. The outer boundary conditions are  $\delta p = 0$  and  $\delta(4\pi r^2 \sigma_{SB} T^4) = \delta L_r$ . The normalization condition  $\max |iT_{l'}| = 1$  is imposed at the surface of the envelope. Because of the density discontinuity at the interfaces between the radiative regions and the convective zone, we need to impose jump conditions for the eigenfunctions, which are for adiabatic oscillations

$$[\xi_r]_-^+ = 0, \quad [\delta p]_-^+ = 0, \quad (15)$$

where  $[f(x)]_-^+ = \lim_{\epsilon \rightarrow +0} (f(x + \epsilon) - f(x - \epsilon))$ . For nonadiabatic calculations, we need additional jump conditions, for which we employ for simplicity

$$[\delta L_{rad}]_-^+ = 0, \quad [\delta s]_-^+ = 0. \quad (16)$$

Truncation of the series expansions of perturbations is inevitable to get a set of linear ordinary differential equations of a finite dimension for numerical calculation. We find that including the first 6 to 8 expansion coefficients is sufficient to obtain reasonable convergence of the eigenfrequencies and eigenfunctions of the modes considered in this paper.

## 4. Numerical Results

### 4.1. Envelope Models

For  $M = 1.4M_\odot$ ,  $R = 10^6 \text{cm}$ , and  $z_b/M_\odot = 1 \times 10^{-10}$  and for the surface chemical composition  $X = 0.7$ ,  $Z = 0.02$ , and  $Z_{CNO} = Z/2$ , we calculated envelope models for  $\dot{M} = 0.1\dot{M}_{Edd}$  and  $\dot{M} = 0.02\dot{M}_{Edd}$ , where  $\dot{M}_{Edd}$  denotes the Eddington accretion rate defined as  $\dot{M}_{Edd} \equiv 4\pi cR/\kappa_e = 1.88 \times 10^{18}(1 + X)^{-1}(R/10^6) \text{g s}^{-1}$  and  $\kappa_e = 0.2(1 + X)$  is the electron scattering opacity. For the mass extent of the convection zone, we assume  $z_e/z_c = 0.01$ . In Table 1, we tabulate several physical quantities characterizing the envelopes, such as  $Ls/L_{Edd}$ , the radial thickness  $\Delta r$  of the envelope, the temperature  $T_b$  at the bottom of the envelope, and  $y_c \equiv z_c/(4\pi R^2)$  for convective models, where  $L_{Edd} \equiv 4\pi cGM/\kappa_e$  is the Eddington luminosity. The

radial extent  $\Delta r$  and the base temperature  $T_b$  of the convective envelope models are larger than those of the radiative models. The base  $z_c$  of the convective zone resides in the mixed hydrogen-helium burning region for the model of  $\dot{M} = 0.1\dot{M}_{Edd}$ , while the base is in the hydrogen-exhausted region for the model of  $\dot{M} = 0.02\dot{M}_{Edd}$ . In Figure 1, we plot the temperature  $T$  versus the column depth  $y \equiv z/(4\pi R^2)$  for  $\dot{M} = 0.1\dot{M}_{Edd}$  in panel (a) and for  $\dot{M} = 0.02\dot{M}_{Edd}$  in panel (b), where the solid lines and the dotted lines are for the radiative and the convective models, respectively. The temperature of the convective models is much higher than that of the radiative models. Both for the radiative and the convective models, the layers below the nuclear burning regions are nearly isothermal. To understand the modal properties of oscillation modes, it is useful to plot the Brunt-Väisälä frequency  $N = \sqrt{-gA}$  with  $g = GM_r/r^2$  and the Lamb frequency  $L_l = \sqrt{l(l+1)}c_s/r$  with  $c_s$  being the sound velocity, where the Schwartzschild discriminant  $A$  is defined as

$$A \equiv \frac{d \ln \rho}{dr} - \frac{1}{\Gamma_1} \frac{d \ln p}{dr} = -\frac{\rho g}{p} \left[ \frac{\chi_T}{\chi_\rho} (\nabla_{ad} - \nabla) + \nabla_\mu \right], \quad (17)$$

where

$$\Gamma_1 = \left( \frac{\partial \ln p}{\partial \ln \rho} \right)_{ad}, \quad \chi_T = \left( \frac{\partial \ln p}{\partial \ln T} \right)_\rho, \quad \chi_\rho = \left( \frac{\partial \ln p}{\partial \ln \rho} \right)_T, \quad \nabla = \frac{d \ln T}{d \ln p}, \quad \nabla_\mu = \frac{d \ln \mu}{d \ln p}, \quad (18)$$

and  $\mu$  is the mean molecular weight. In Figure 2,  $N^2$  and  $L_l^2$  with  $l = 1$  are plotted versus  $y$  for the models of  $\dot{M} = 0.1\dot{M}_{Edd}$  in panel (a) and for the models of  $\dot{M} = 0.02\dot{M}_{Edd}$  in panel (b), where the solid lines and the dotted lines indicate respectively the radiative and the convective models, and  $N^2$  and  $L_l^2$  are normalized by  $GM/R^3$ . Note that we have  $N^2 < 0$  in convective regions. Figure 3 gives the mean molecular weight  $\mu$  as a function of  $y$ , where the solid line and the dashed line are for the radiative and the convective models of  $\dot{M} = 0.1\dot{M}_{Edd}$ , and the dotted line and the dash-dotted line are for the radiative and the convective models of  $\dot{M} = 0.02\dot{M}_{Edd}$ . Figure 3 shows that the spiky or needle-like features found in the Brunt-Väisälä frequency is produced by extremely steep increase of the mean molecular weight  $\mu$  with increasing  $y$  in the active nuclear burning regions.

## 4.2. Eigenfrequencies

It is now well known that the corotating-frame oscillation frequency  $\omega \equiv \sigma + m\Omega$  of the  $r$ -modes in non-isentropic stars is in the limit of  $\Omega \rightarrow 0$  asymptotic to the frequency given by

$$\omega = 2m\Omega/[l'(l' + 1)], \quad (19)$$

and that for a given combination of  $(m, l', \Omega)$  there exist the fundamental  $r$ -mode with no radial nodes of the eigenfunction  $iT_{l'}$  and its overtones (see, e.g., Yoshida & Lee 2001). Note that the inertial-frame oscillation

Table 1. Physical parameters of the envelope models

$\dot{M}/\dot{M}_{Edd}$	$L_s/L_{Edd}$	$\Delta r$ (cm)	$T_b$ (K)	$y_c$ (g/cm <sup>2</sup> )	comment
0.1	2.70E−3	3.17E3	4.02E8	...	radiative
	1.75E−2	4.55E3	9.70E8	1.50E8	convective
0.02	5.26E−4	2.61E3	2.01E8	...	radiative
	4.34E−1	6.82E3	1.45E9	1.65E8	convective

frequency  $\sigma$  of the  $r$ -modes is negative for positive  $m$ , indicating the modes are prograde observed in an inertial frame. In this paper, we calculate the fundamental  $r$ -modes of  $l' = |m|$ ,  $|m| + 1$ ,  $|m| + 2$ ,  $|m| + 3$  for  $m = 1$  and  $m = 2$  at several values of  $\Omega$  for the envelope models. In Figure 4, the oscillation frequencies  $\omega/2\pi$  for the radiative models are plotted versus  $\Omega/2\pi$  for  $\dot{M} = 0.1\dot{M}_{Edd}$  in panel (a) and for  $\dot{M} = 0.02\dot{M}_{Edd}$  in panel (b), where the solid lines with open symbols and those with filled symbols are for the modes of  $m = 1$  and  $m = 2$ , respectively, and the circles, squares, triangles, and diamonds indicate the  $r$ -modes of  $l' = |m|$ ,  $|m| + 1$ ,  $|m| + 2$ , and  $|m| + 3$ , respectively. As  $\Omega$  is increased, the frequency  $\omega$  of the  $r$ -modes of  $l' > |m|$  deviates appreciably from the asymptotic frequency (19), and becomes almost insensitive to  $\Omega$ , gathering in a frequency range of  $\omega/2\pi \lesssim 10\text{Hz}$ , at rapid rotation rates. For convenience, we have tabulated in Table 2 the oscillation frequency of the fundamental  $r$ -modes of  $m = 1$  and 2 for  $\Omega/2\pi = 300\text{ Hz}$  and  $600\text{ Hz}$  for the radiative envelope models. Table 2 clearly shows that the  $r$ -mode frequency of the radiative models is also dependent on the mass accretion rates and is practically independent of the spin frequency at rapid rotation rates for  $l' > |m|$ . As shown in the next subsection, the amplitudes of the  $r$ -modes at rapid rotation rates are strongly confined in the equatorial regions of the star, in which the Coriolis parameter  $2\Omega \sin \hat{\theta}$  with  $\hat{\theta}$  being the latitude has small values. The modal properties found for the  $r$ -modes of a thin spherical shell at rapid rotation rates are quite similar to those of the low frequency equatorial waves in the ocean of the earth (e.g., Pedlosky 1987).

Since in the propagation zone of the  $r$ -modes the pressure scale height  $H_p \approx y/\rho$  of the convective models is larger than that of the radiative models because of higher envelope temperature of the former, the oscillation frequency  $\omega$  of the  $r$ -modes in the convective models is increased compared to that in the radiative models (see the dispersion relation given in Discussion). This increase in  $\omega$  for the convective models in turn leads to a *decrease* in the inertial-frame oscillation frequency  $|\sigma|$ , compared to that for the radiative models. In Figure 5, the relative difference  $f$  of the oscillation frequency of the fundamental  $r$ -modes between the radiative and the convective models is plotted versus  $\sigma_{rad}/2\pi$  for  $\dot{M}/\dot{M}_{Edd} = 0.1$  in panel (a) and for  $\dot{M}/\dot{M}_{Edd} = 0.02$  in panel (b), where

$$f = -(\sigma_{conv} - \sigma_{rad})/\sigma_{rad}, \quad (20)$$

and  $\sigma_{conv}$  and  $\sigma_{rad}$  are the oscillation frequencies for the convective and the radiative envelope models, respectively, and the solid lines with open symbols and those with filled symbols are for the  $r$ -modes of  $m = 1$  and  $m = 2$ , respectively, and the circles, squares, triangles, and diamonds indicate the  $r$ -modes of  $l' = |m|$ ,  $|m| + 1$ ,  $|m| + 2$ , and  $|m| + 3$ , respectively. Note that the relative frequency difference  $f$  for the  $r$ -modes of  $(m, l') = (1, 1)$  is larger than 0.1, and is outside the range employed for the figure. As  $-\sigma_{rad}$  is increased,  $f$  for the fundamental  $r$ -mode of given  $(m, l')$  decreases gradually after passing a maximum. We find that the relative differences  $f$  at  $|\sigma_{rad}|/2\pi \sim 300\text{Hz}$  for  $m = 1$  and at  $|\sigma_{rad}|/2\pi \sim 600\text{Hz}$  for  $m = 2$ , for example, have similar values, and that  $f$  for given  $m$  and  $\Omega$  becomes smaller for larger values of  $l'$ . If we compare the relative differences  $f$  calculated here with the frequency drifts observed in burst oscillations in X-ray bursters, we find that the fundamental  $r$ -modes of  $l' > |m| + 1$  produce relative differences  $f$  consistent with observed frequency drifts at  $|\sigma|/2\pi \sim 300\text{Hz}$  for  $m = 1$  or at  $|\sigma|/2\pi \sim 600\text{Hz}$  for  $m = 2$ , although the differences  $f$  for the  $r$ -modes of  $l' = |m|$  are too large to be reconciled with the observations for the models used in this paper. If the star is rotating as rapidly as  $\Omega/2\pi \sim 600\text{Hz}$ ,  $f$  for the  $m = 1$   $r$ -modes also becomes consistent with observed values, which suggests the possibility that the burst QPO near  $600\text{Hz}$  could be produced by the  $r$ -modes of  $m = 1$ . We also note that to obtain values of  $f$  as small as  $\sim 0.001$  we need to consider the  $r$ -modes that have the index  $l'$  much larger than  $|m|$ .

Although the  $r$ -modes in the radiative models are all pulsationally stable for the mass accretion rates considered in this paper (see Strohmayer & Lee 1996), the fundamental  $r$  modes in the convective models

are driven unstable by strong nuclear burning in the convective zone. In Figure 6, the growth timescale  $\tau_{growth} \equiv -1/\sigma_I$  of the  $r$ -modes in the convective models is plotted as a function of  $\Omega/2\pi$  for  $\dot{M} = 0.1\dot{M}_{Edd}$  in panel (a) and for  $\dot{M} = 0.02\dot{M}_{Edd}$  in panel (b), where  $\sigma_I$  is the imaginary part of the eigenfrequency  $\sigma$ , and the solid lines with open symbols and those with filled symbols are for the modes of  $m = 1$  and  $m = 2$ , respectively, and the circles, squares, and triangles indicate the  $r$ -modes of  $l' = |m|$ ,  $|m| + 1$ , and  $|m| + 2$ , respectively.  $\tau_{growth}$ 's for  $\dot{M} = 0.02\dot{M}_{Edd}$  are by about three order of magnitude shorter than those for  $\dot{M} = 0.1\dot{M}_{Edd}$ , because the envelope temperature of the former is much higher than that of the latter. Note that  $\tau_{growth}$  becomes almost insensitive to  $\Omega$  for rapid rotation rates.

### 4.3. Eigenfunctions

The expansion coefficients  $iT_{l'}$  and  $H_l$  of the fundamental  $r$ -modes of  $(m, l') = (2, 3)$  at  $\bar{\Omega} = \Omega/\sqrt{GM/R^3} = 0.1$  are shown versus the column depth  $y$  for the models with  $\dot{M} = 0.1\dot{M}_{Edd}$  in Figure 7, and those of  $(m, l') = (1, 1)$  for the models with  $\dot{M} = 0.02\dot{M}_{Edd}$  in Figure 8, where the panels (a) and (b) are for the radiative models and the panels (c) and (d) for the convective models, and the amplitude normalization is given by  $\max |iT_{l'}| = 1$  at the surface. As shown by Figure 7, the component  $iT_{l'=|m|+1}$  of the  $r$ -mode at  $\bar{\Omega} = 0.1$  is no longer dominant over the other components of  $iT_{l'}$  and  $H_l$ . This is also the case for the component  $iT_{l'=|m|}$  of the  $r$ -mode of  $(m, l') = (1, 1)$  shown in Figure 8. The modal properties of the modes at  $\bar{\Omega} = 0.1$  are thus quite different from the properties found for the  $r$ -modes in the limit of  $\bar{\Omega} \rightarrow 0$ , for which the toroidal component  $iT_{l'=|m|+1}$  (or  $iT_{l'=|m|}$ ) is dominant over the other components  $iT_{l'}$ ,  $H_l$ , and  $S_l$ . This becomes clear if we show the  $\theta$  dependence of the eigenfunctions  $\xi_\theta$  and  $\xi_\phi$ , for example. To do so, we introduce the functions  $X_\theta(r, \theta, \phi)$  and  $X_\phi(r, \theta, \phi)$  defined as

$$X_\theta(r, \theta, \phi) = \Re [\xi_\theta(r, \theta, \phi, t)e^{-i\sigma t}/r], \quad (21)$$

$$X_\phi(r, \theta, \phi) = -\Re [i\xi_\phi(r, \theta, \phi, t)e^{-i\sigma t}/r], \quad (22)$$

and, for  $r = R$  and  $\phi = 0$ , we plot the functions  $X_\theta$  (solid lines) and  $X_\phi$  (dotted lines) versus  $\cos \theta$  for the fundamental  $r$ -modes of  $(m, l') = (1, 1)$ ,  $(1, 2)$ , and  $(1, 3)$  in Figure 9 and for those of  $(m, l') = (2, 2)$ ,  $(2, 3)$ , and  $(2, 4)$  in Figure 10, where the radiative model of  $\dot{M} = 0.02\dot{M}_{Edd}$  has been used for the mode calculation, and the amplitude normalization is given by  $\max |iT_{l'}| = 1$  at the surface. Here, in each figure the panels on the left-hand-side are for  $\bar{\Omega} = 0.01$ , and those on the right-hand-side are for  $\bar{\Omega} = 0.1$ . Although the  $r$ -modes have large amplitudes at the poles at  $\bar{\Omega} = 0.01$ , the amplitudes of the modes at  $\bar{\Omega} = 0.1$  become well confined into the equatorial regions of the star, and have effectively no amplitudes at the poles. Note that the parity of the function  $X_\theta e_\theta$  becomes the same as that of  $X_\phi$  with respect to  $\cos \theta$ .

It may be instructive to give a plot of  $\delta L_r$  for the  $r$ -modes considered in this paper, although nonadiabatic calculation is not necessarily quite reliable for the convective models because of our lack of knowledge concerning the interaction between pulsations and convection, and because of somewhat adhoc way of construction of the models. For the convective model of  $\dot{M}/\dot{M}_{Edd} = 0.1$ , Figure 11 shows the expansion coefficients  $\Re(\delta L_{r,l}/L_s)$  as a function of  $y$  for the fundamental  $r$ -mode of  $(m, l') = (2, 3)$  in panel (a) and for that of  $(m, l') = (2, 5)$  in panel (b) at  $\bar{\Omega} = 0.1$ , where the solid, dotted, dashed, and dash-dotted lines are for the expansion coefficients with  $l = |m|$ ,  $|m| + 2$ ,  $|m| + 4$ , and  $|m| + 6$ , respectively, and the amplitude normalization is given by  $\max |iT_{l'}| = 1$  at the surface. Figure 12 illustrates  $\Re(\delta L_r/L_s)$  versus  $\cos \theta$ , where the solid and the dotted lines respectively designate the  $r$ -modes of  $(m, l') = (2, 3)$  and  $(m, l') = (2, 5)$  at  $\bar{\Omega} = 0.1$ , and we have assumed  $r = R$  and  $\phi = 0$ . From Figures 11 and 12, we find that  $\Re(\delta L_{r,l}/L_s)$  at the surface has large amplitudes, comparable to  $\max |iT_{l'}|$ , in the equatorial regions, and



that, although  $\Re(\delta L_r/L_s)$  of the  $r$ -mode of  $(m, l') = (2, 3)$  does not change its sign as a function of  $\cos \theta$ ,  $\Re(\delta L_r/L_s)$  of the  $r$ -mode of  $(m, l') = (2, 5)$  changes its sign at a middle latitude, which may result in a reduction of the detectability of the signals produced by the mode. Note that the  $r$ -modes of  $(m, l') = (2, 3)$  and  $(m, l') = (2, 5)$  are even modes, and the perturbation  $\delta L_r/L_s$  is symmetric about the equator. On the other hand, the odd  $r$ -modes of  $l' = |m|, |m| + 2, \dots$  have the eigenfunctions antisymmetric about the equator.

## 5. Discussion

Erecting at the equator a cartesian coordinate system in which the coordinates  $x$ ,  $y$ , and  $z$  are directed to the east, the north, and the zenith, respectively, and applying the  $\beta$ -plane approximation at the origin, we may obtain the dispersion relation for equatorial waves given by (Pedlosky 1987)

$$\lambda \bar{\omega}^2 + \frac{\bar{k}}{\bar{\omega}} - \bar{k}^2 = (2j + 1)\sqrt{\lambda}, \quad (23)$$

where  $\bar{k}$  is the dimensionless wavenumber in the  $x$  direction, and  $\lambda$  is the separation constant between the horizontal and vertical momentum equations, and the velocity perturbation  $v'_y$ , for example, have been assumed to have the form given by  $e^{i(kx + \omega t)}\Psi(y)G(z)$ . Here, the separation constant  $\lambda$  is determined by the vertical-structure equation that governs the function  $G(z)$ , and the non-negative-integer  $j$  comes from the normal mode equation for  $v'_y$ , for which the function  $\Psi(y)$  is shown to be proportional to  $e^{-\eta^2/2}H_j(\eta)$ , where  $H_j(\eta)$  is the Hermite polynomial and  $\eta = \sqrt{\lambda}y/L_e$  (Pedlosky 1987). In the dispersion relation, the dimensionless oscillation frequency  $\bar{\omega}$  and the wavenumber  $\bar{k}$  in the  $x$  direction are normalized as

$$\bar{\omega} = \omega/(\beta_0 L_e), \quad \bar{k} = L_e k, \quad (24)$$

where  $\beta_0 = 2\Omega/R$ , and

$$L_e = \sqrt{N_0 D / \beta_0} \quad (25)$$

is the equatorial Rossby internal-deformation radius, and  $N_0$  is the characteristic value of the Brunt-Väisälä frequency,  $D$  is the depth of the atmosphere or the ocean (Pedlosky 1987). Rewriting the dispersion relation using dimensional  $\omega$  and  $k$ , and taking the low frequency limit, we obtain

$$\frac{N_0 D}{\omega} k - \frac{N_0 D}{\beta_0} k^2 = (2j + 1)\sqrt{\lambda}, \quad (26)$$

which can be solved for  $\omega$  to give

$$\omega = \frac{N_0 D k}{(2j + 1)\sqrt{\lambda} + N_0 D k^2 / \beta_0} \sim \frac{m N_0 (D/R)}{(2j + 1)\sqrt{\lambda} + m^2 N_0 (D/R) / 2\Omega}, \quad (27)$$

where we have assumed  $k \sim m/R$  with  $m$  being an integer corresponding to the azimuthal wave number. Note that the oscillation frequency is proportional to the depth  $D$  of the atmosphere or the ocean, and  $D/R \ll 1$ . In the limit of  $\Omega \rightarrow 0$ , we obtain

$$\omega \rightarrow 2\Omega/m, \quad (28)$$

and we obtain at rapid rotation speeds

$$\omega \sim \frac{m N_0 (D/R)}{(2j + 1)\sqrt{\lambda}}, \quad (29)$$

which does not depend on  $\Omega$ . If we regard  $D$  and  $N_0$  as the pressure-scale-height  $H_p$  and the characteristic value of  $N$  found in the  $r$ -mode propagation region, the dispersion relation given above describes qualitatively well the  $\Omega$  dependence of the  $r$ -mode frequency  $\omega$  obtained in this paper. The quantity  $N_0(D/R)$  in equation (29) may depend on parameters such as the surface gravity  $g = GM/R^2$ , the radius  $R$ , and the mass accretion rate, and extensive model calculations would be required to see how the quantity  $N_0(D/R)$  depends on the parameters. Note that the equatorial waves have large amplitudes at the equatorial regions but vanishing amplitudes at the poles as indicated by the function  $\Psi(y) \propto e^{-\eta^2/2} H_j(\eta)$ , the properties of which are similar to those of the  $r$ -modes found in this paper.

## 6. Conclusion

In this paper, we calculated the  $r$ -modes propagating in mass-accreting, nuclear burning, and geometrically thin envelopes on the surface of rotating neutron stars. In steady state approximation, we constructed thin envelope models which are fully radiative or have a convective region. The radiative and the convective models were intended to represent envelope structures in a late phase and in an early phase of an X-ray burst, respectively. The convective models have higher temperature and larger geometrical thickness than the corresponding radiative models. We find that the corotating-frame oscillation frequency  $\omega$  of the fundamental  $r$ -modes of  $(m, l')$ , which is asymptotic to  $\omega = 2m\Omega/[l'(l' + 1)]$  when  $\Omega \rightarrow 0$ , becomes essentially insensitive to  $\Omega$  and gathers in a frequency range of  $\omega/2\pi \lesssim 10\text{Hz}$  at rapid rotation rates. It is also found that the amplitudes of the  $r$ -modes at rapid rotation rates become well confined to the equatorial regions of the star. Although the fundamental  $r$ -modes of the radiative envelope models are all pulsationally stable for the mass accretion rates considered in this paper, the  $r$ -modes of the convective models are driven unstable by nuclear burning in the convection zone.

It is found that the inertial-frame oscillation frequency  $|\sigma|$  of the  $r$ -modes of given  $(m, l', \Omega)$  for the convective models becomes lower than that for the corresponding radiative models. In order to estimate possible magnitudes of the relative frequency changes of the  $r$ -modes during an X-ray burst, we calculated  $f = -(\sigma_{conv} - \sigma_{rad})/\sigma_{rad}$  as a function of  $\Omega$ , where  $\sigma_{rad}$  and  $\sigma_{conv}$  are the oscillation frequencies of the fundamental  $r$ -modes in the radiative and the convective envelope models, respectively. We find that, if we consider the burst oscillations of  $|\sigma_{rad}|/2\pi \sim 300\text{Hz}$  or  $|\sigma_{rad}|/2\pi \sim 600\text{Hz}$ , the fundamental  $r$ -modes of  $l' > |m| + 1$  with  $m = 1$  or  $m = 2$  can produce the relative frequency changes  $f$  consistent with the observed relative frequency drifts of less than  $\sim 1\%$ , although we need to consider the  $r$ -modes of  $l'$  much larger than  $|m|$  for values of  $f$  as small as  $\sim 0.001$ . We also find that  $f$  for the  $\dot{M} = 0.02\dot{M}_{Edd}$  models is larger than that for the  $\dot{M} = 0.1\dot{M}_{Edd}$  models, which may reflect the properties of nuclear flashes dependent on the mass accretion rates (see, e.g., Fujimoto, Hanawa, & Miyaji 1981) and could be tested observationally. Considering that the fundamental  $r$ -modes in the convective models are driven unstable by nuclear burning in the convective zone, it is tempting to postulate that the burst oscillations observed in X-ray bursts are produced by the  $r$ -modes of low indices  $(m, l')$  that are excited in the early phase of the nuclear flash and survive until the tail, changing the frequency slightly according to the changes in the envelope structure. The  $r$ -mode scenario is consistent with the observations that indicate the existence of two frequencies separated by a few Hz, since the fundamental  $r$ -modes of different  $l'$ 's for a given  $m$  could be excited simultaneously in a burst to have similar oscillation frequencies for rapidly rotating neutron stars. The temporal frequency decrease observed in the tail of bursts from 4U 1636-53 (Strohmayer 1999) and KS 1731-260 (Muno et al 2000) may be attributable to switching of the  $r$ -modes observable to us from those of  $(m, l'_1)$  to  $(m, l'_2)$  where  $l'_1 > l'_2$  for frequency decrease. The mode switching will cause discontinuous

frequency changes and could be tested by a close observation of the frequency evolution. To make possible the close comparison between observations and the  $r$ -mode scenario for burst oscillations, however, it is definitely necessary to use more realistic envelope models obtained from time-dependent flash calculation with a reliable treatment of the convection zone.

Recently, Chakrabarty et al (2003) reported the detection of quasi-periodic oscillations in X-ray bursts of the millisecond pulsar SAX J1808.4-3658, showing that the oscillation frequencies agree quite well with the spin frequency of the star. The time evolution of the burst oscillation frequencies, however, was found quite different from that in other X-ray bursters that show burst oscillations. The frequency drift  $\Delta\nu/\nu \sim 0.01$  is among the largest observed in any neutron star. The drift time scale is an order of magnitude faster than in the other neutron stars, and the oscillation frequency overshoots the spin frequency, reaching the maximum during the burst rise. The burst oscillations found in the pulsar are inconsistent with both the contracting shell model with angular momentum conservation and the  $r$ -mode scenario. A key factor for the burst oscillations in the star may be a strong magnetic field inferred from the existence of coherent X-ray pulsations in non-burst phases, since the strong magnetic field has significant effects both on the modal properties of waves propagating in the surface layers and on the way of nuclear burning on the surface of the star.

## REFERENCES

- Arnett, W.D., & Truran, J.W. 1969, ApJ, 157, 339
- Beaudet, G., Petrosian, V., & Slapeter, E.E. 1967, ApJ, 150, 979
- Canuto, V. 1970, ApJ, 159, 641
- Chakrabarty, D., Morgan, E.H., Muno, M.P., Galloway, D.K., Wijnands, R., van der Klis, M., & Markwardt, C.B. 2003, Nature, 424, 42
- Cox, A.N., & Stewart, J.N. 1970, ApJS, 19, 243
- Cumming, A., & Bildsten, L. 2000, ApJ, 544, 453
- Cumming, A., Morsink, S.M., Bildsten, L., Friedman, J.L., & Holz, D.E. 2001, ApJ, 564, 343
- Fowler, W.A., Caughlan, G.R., & Zimmerman, B.A. 1975, ARA&A, 13, 69
- Fujimoto, M.Y., Hanawa, T., & Miyaji, S. 1981, ApJ, 246, 267
- Gilles, A.B., Hill, K.M., Strohmayer, T.E., & Cummings, N. 2002, ApJ, 568, 279
- Galloway, D.K., Chakrabarty, D., Muno, M.P., & Savov, P. 2001, ApJ, 549, L85
- Greenspan, H.P. 1968, The Theory of Rotating Fluids, Cambridge University Press
- Hanawa, T., & Sugimoto, D. 1982, PASJ, 34, 1
- Heyl, J.S. 2001, astro-ph/0108450
- Hubbard, W.B., & Lampe, M. 1969, ApJ, 156, 795
- Lee, U., & Saio, H. 1987, MNRAS, 225, 643

- Lee, U., & Saio, H. 1993, MNRAS, 261, 415
- Lee, U., & Baraffe, I. 1995, A&A, 301, 419
- McDermott, P.N., & Taam, R.E. 1987, ApJ, 318, 278
- Miller, M.C. 2000, ApJ, 531, 458
- Muno, M.P., Fox, D.W., Morgan, E.H., & Bildsten, L. 2000, ApJ, 542, 1016
- Muno, M.P., Chakrabarty, D., Galloway, D.K., & Psaltis, D. 2002, ApJ, 580, 1048
- Muno, M.P., Özel, E., & Chakrabarty, D. 2002, ApJ, 581, 550
- Paczynski, B. 1970, Acta Astron., 20, 40
- Patterson, J.R., Winkler, H., & Zaidins, C.S. 1969, ApJ, 157, 367
- Pedlosky, J. 1987, Geophysical Fluid Dynamics, 2ed. Springer-Verlag, New York
- Reeves, H. 1965, in Stellar Structure, ed. L.H. Aller & D.B. McLaughlin (Chicago: Univ. Chicago Press), 113
- Salpeter, E.E., & Van Horn, H.M. 1969, ApJ, 155, 183
- Spitkovsky, A., Levin, Y., & Ushomirsky, G. 2002, ApJ, 566, 1018
- Strohmayer, T.E., & Lee, U. 1996, ApJ, 467, 773
- Strohmayer, T.E., Zhang, W., Swank, J.H., Smale, A., Titarchuk, L., Day, C., & Lee, U. 1996, ApJ, 469, L9
- Strohmayer, T.E., Jahoda, K., Giles, B.A., & Lee, U. 1997, ApJ, 486, 355
- Strohmayer, T.E., Zhang, W., Swank, J.H., & Lapidus, I. 1998, ApJ, 503, L147
- Strohmayer, T.E., 1999, ApJ, 523, L51
- Strohmayer, T.E., & Bildsten, L. 2003, in Compact Stellar X-Ray Sources, eds. W.H.G. Lewin and M. van der Klis, Cambridge University Press
- Wallace, R.K., & Woosley, S.E. 1981, ApJS, 45, 389
- Yoshida, S., & Lee, U. 2001, ApJS, 129, 353

Table 2. Oscillation frequency  $\nu_{l'}^a = \omega_{rad}/2\pi$  of the fundamental  $r$ -modes of the radiative envelopes

$\dot{M}/\dot{M}_{Edd}$	$m$	$\Omega/2\pi^a$	$\nu_{l'= m }$	$\nu_{l'= m +1}$	$\nu_{l'= m +2}$	$\nu_{l'= m +3}$
0.1	1	300	128.4	11.51	7.076	5.160
		600	188.1	11.52	7.002	5.062
	2	300	113.6	21.79	13.61	9.995
		600	172.6	22.45	13.75	9.974
0.02	1	300	112.4	8.543	5.219	3.784
		600	163.8	8.558	5.193	3.800
	2	300	101.2	16.42	10.15	7.404
		600	152.1	16.78	10.24	7.469

<sup>a</sup>Frequencies are given in Hz

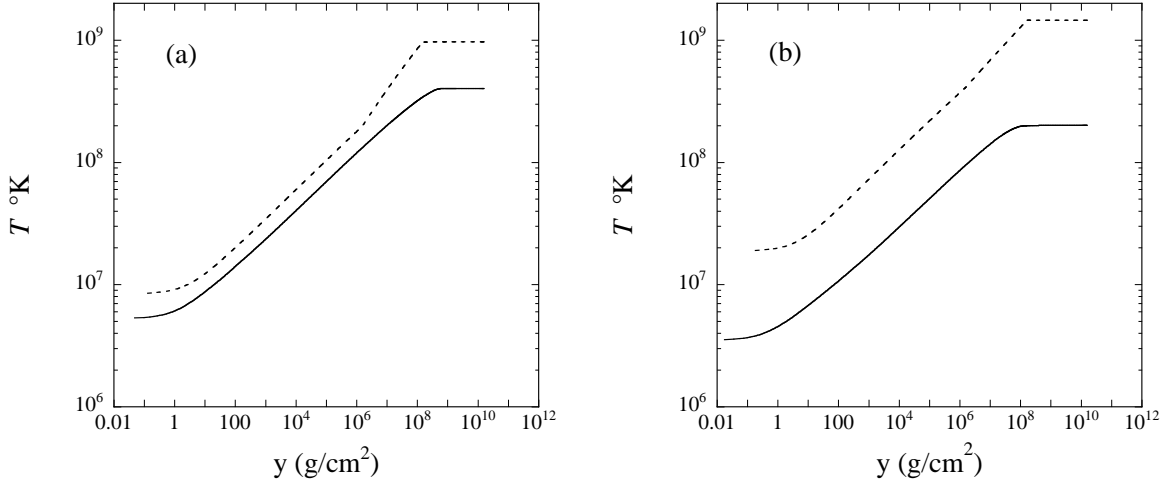


Fig. 1.— Temperature  $T$  as a function of the column depth  $y$  for  $\dot{M} = 0.1\dot{M}_{Edd}$  in panel (a) and for  $\dot{M} = 0.02\dot{M}_{Edd}$  in panel (b), where the solid lines and the dotted lines are for the radiative and the convective models, respectively.

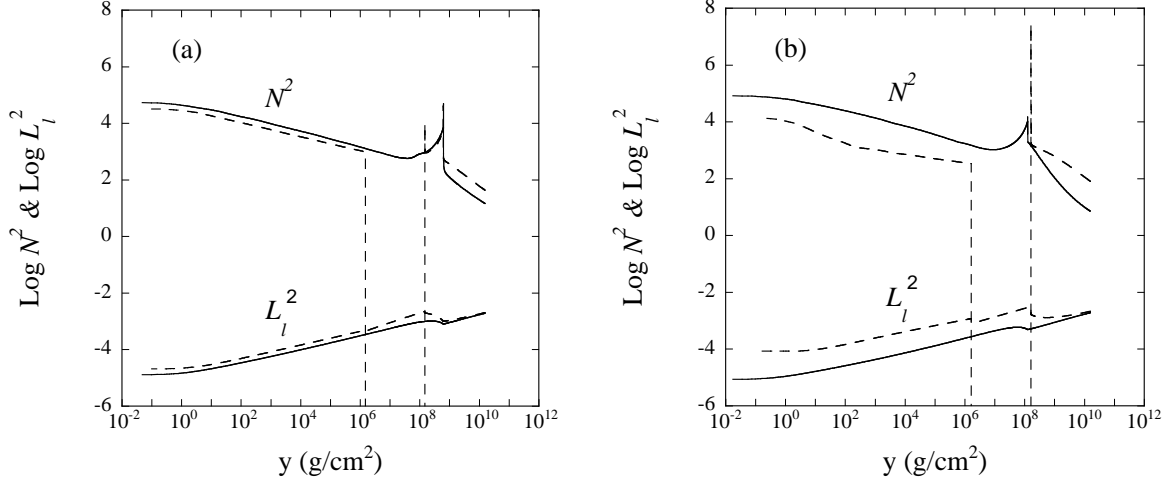


Fig. 2.— Propagation diagram for the envelope models, where the square of Brunt-Väisälä frequency  $N$  and Lamb frequency  $L_l$  with  $l = 1$  are displayed versus the column depth  $y$  for the radiative models (solid lines) and the convective models (dashed lines).  $N^2$  and  $L_l^2$  are normalized by  $GM/R^3$  with  $M$  and  $R$  being the mass and the radius of the neutron star. Panels (a) and (b) are for the cases of  $\dot{M}/\dot{M}_{Edd} = 0.1$  and  $0.02$ , respectively.

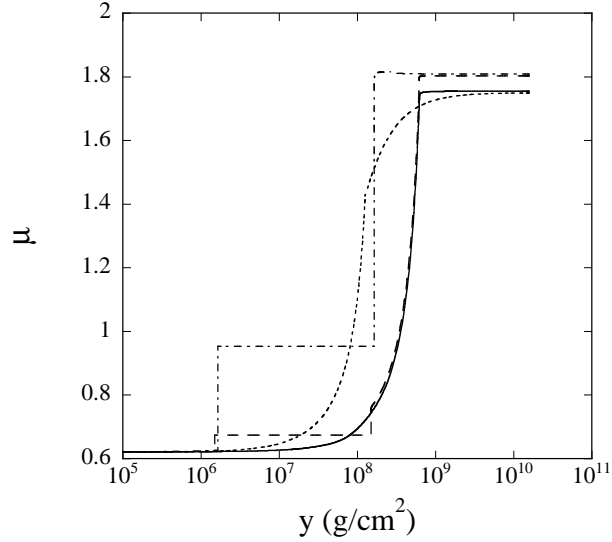


Fig. 3.— Mean molecular weight  $\mu$  as a function of the column depth  $y$  for the radiative (solid line) and the convective (dashed line) models of  $\dot{M}/\dot{M}_{Edd} = 0.1$  and the radiative (dotted line) and the convective (dash-dotted line) models of  $\dot{M}/\dot{M}_{Edd} = 0.02$ .

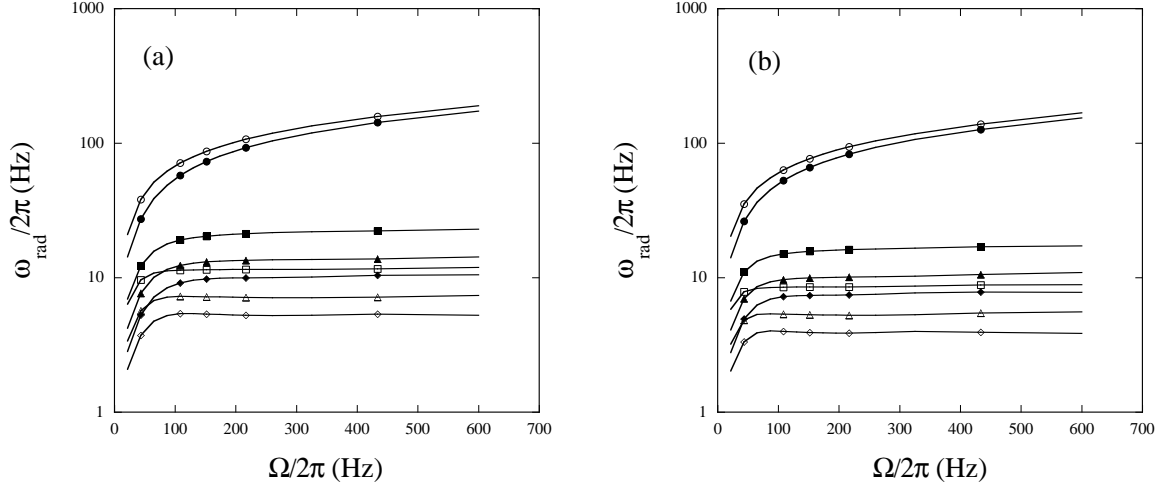


Fig. 4.— Oscillation frequencies  $\omega$  of the fundamental  $r$ -modes of the radiative envelope models are given versus  $\Omega/2\pi$  for  $\dot{M}/\dot{M}_{\text{Edd}} = 0.1$  in panel (a) and for  $\dot{M}/\dot{M}_{\text{Edd}} = 0.02$  in panel (b), where the solid lines attached by open symbols and those by filled symbols are for  $m = 1$  and  $m = 2$ , respectively, and the circles, squares, triangles, and diamonds indicate the  $r$ -modes of  $l' = |m|$ ,  $|m| + 1$ ,  $|m| + 2$ ,  $|m| + 3$ , respectively.

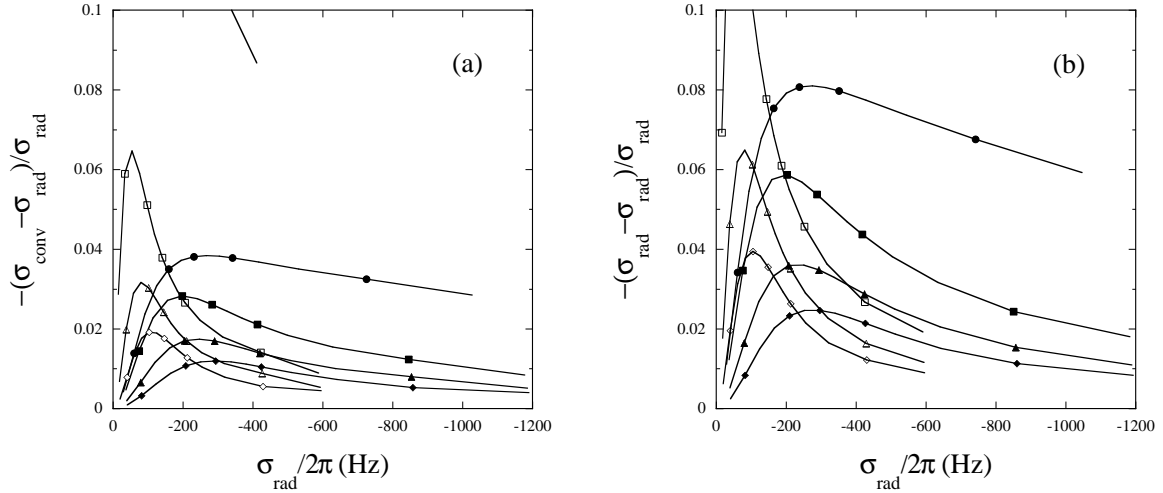


Fig. 5.— Relative frequency differences  $f \equiv -(\sigma_{\text{conv}} - \sigma_{\text{rad}})/\sigma_{\text{rad}}$  of the fundamental  $r$ -modes between the radiative and the convective envelope models are plotted versus  $\sigma_{\text{rad}}/2\pi$  for  $\dot{M}/\dot{M}_{\text{Edd}} = 0.1$  in panel (a) and for  $\dot{M}/\dot{M}_{\text{Edd}} = 0.02$  in panel (b), where the solid lines attached by open symbols and those by filled symbols are for  $m = 1$  and  $m = 2$ , respectively, and the circles, squares, triangles, and diamonds indicate the  $r$ -modes of  $l' = |m|$ ,  $|m| + 1$ ,  $|m| + 2$ ,  $|m| + 3$ , respectively. Here,  $\sigma_{\text{rad}}$  and  $\sigma_{\text{conv}}$  are the inertial-frame oscillation frequencies of the  $r$ -modes in the radiative and the convective models, respectively.

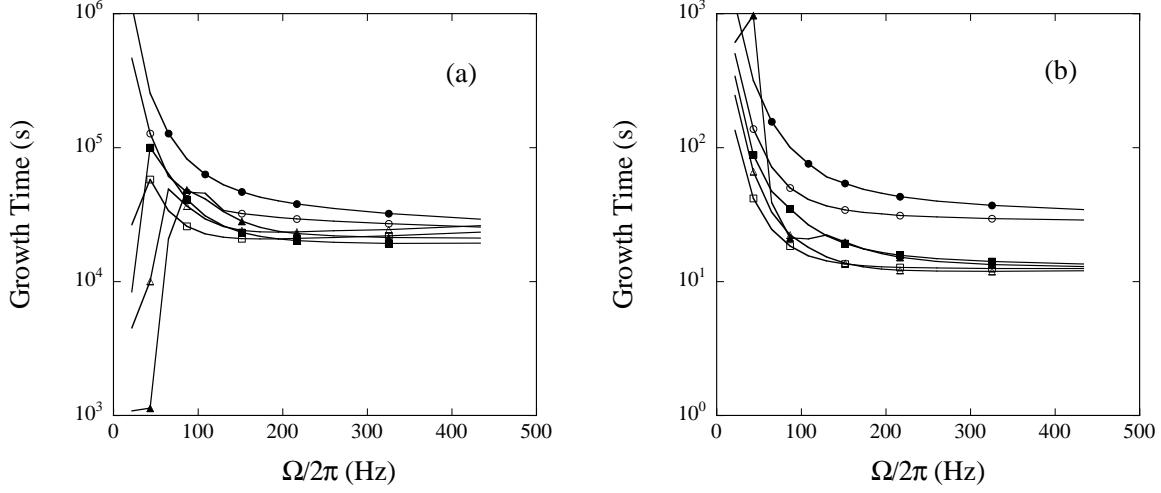


Fig. 6.— Growth time-scales  $\tau_{growth} \equiv -1/\sigma_I$  of the fundamental  $r$ -modes of the convective envelope models are plotted versus  $\Omega/2\pi$  for  $\dot{M}/\dot{M}_{Edd} = 0.1$  in panel (a) and for  $\dot{M}/\dot{M}_{Edd} = 0.02$  in panel (b), where the solid lines attached by open symbols and those by filled symbols are for  $m = 1$  and  $m = 2$ , respectively, and the circles, squares, and triangles indicate the  $r$ -modes of  $l' = |m|$ ,  $|m| + 1$ , and  $|m| + 2$ , respectively. Here,  $\sigma_I$  is the imaginary part of the eigenfrequency of the  $r$ -modes.

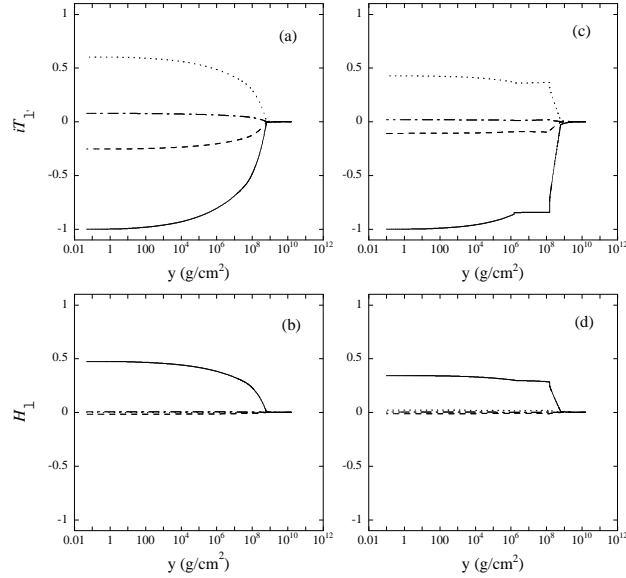


Fig. 7.— Expansion coefficients  $iT_{l'}$  and  $H_l$  of the fundamental  $r$ -mode of  $(m, l') = (2, 3)$  at  $\bar{\Omega} = 0.1$  are given versus the column depth  $y$  for  $\dot{M}/\dot{M}_{Edd} = 0.1$ , where the solid, dotted, dashed, and dash-dotted lines indicate the coefficients associated with  $l = l' - 1 = |m|$ ,  $|m| + 2$ ,  $|m| + 4$ , and  $|m| + 6$ , respectively, and the amplitude normalization is given by  $\max |iT_{l'}| = 1$  at the surface. Here, panels (a) and (b) are for the radiative models, and panels (c) and (d) are for the convective models.



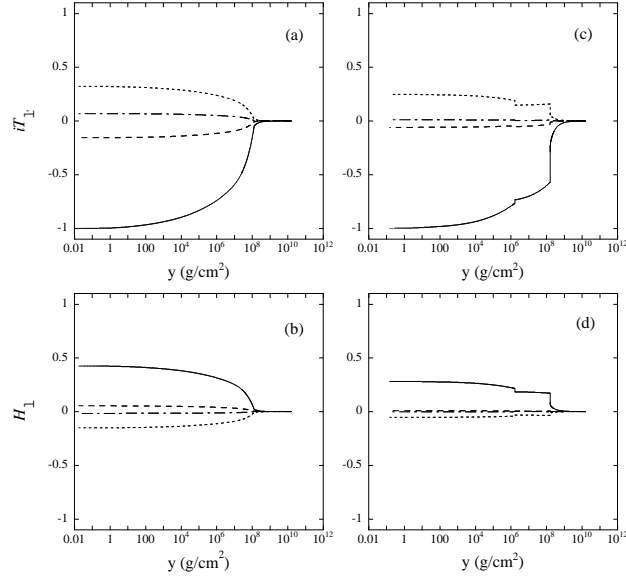


Fig. 8.— Expansion coefficients  $iT_{l'}$  and  $H_l$  of the fundamental  $r$ -mode of  $(m, l') = (1, 1)$  at  $\bar{\Omega} = 0.1$  are given versus the column depth  $y$  for  $\dot{M}/\dot{M}_{Edd} = 0.02$ , where the solid, dotted, dashed, and dash-dotted lines indicate the coefficients associated with  $l' = l - 1 = |m|$ ,  $|m| + 2$ ,  $|m| + 4$ , and  $|m| + 6$ , respectively, and the amplitude normalization is given by  $\max |iT_{l'}| = 1$  at the surface. Here, panels (a) and (b) are for the radiative models, and panels (c) and (d) are for the convective models.

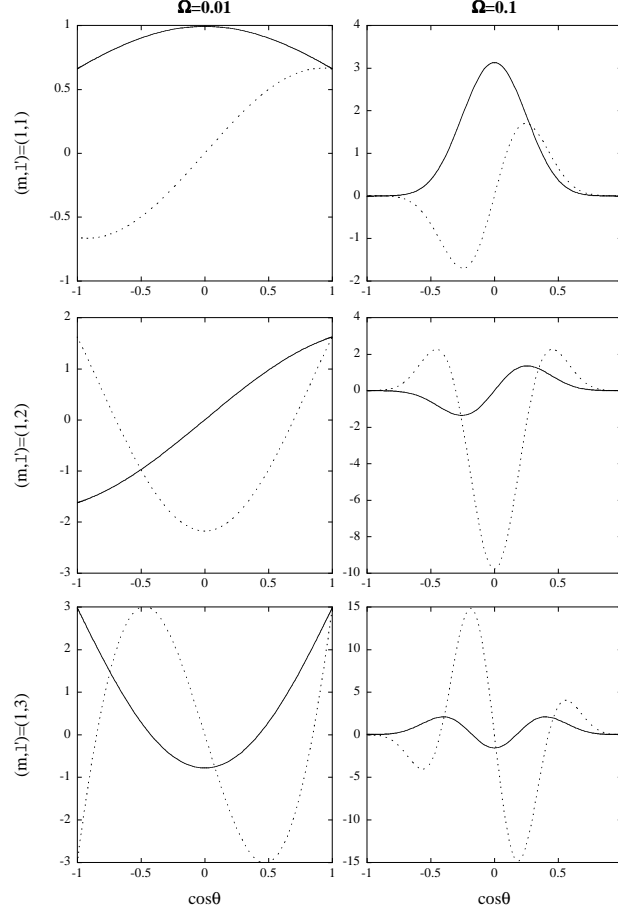


Fig. 9.— Functions  $X_\theta(r, \theta, \phi)$  and  $X_\phi(r, \theta, \phi)$  for  $r = R$  and  $\phi = 0$  are plotted versus  $\cos\theta$  for the fundamental  $r$ -modes of  $l' = |m|$ ,  $|m| + 1$ , and  $|m| + 2$  for  $m = 1$ , where the solid lines and the dotted lines denote the functions  $X_\theta$  and  $X_\phi$ , respectively, and the radiative model with  $\dot{M}/\dot{M}_{Edd} = 0.02$  has been used for the mode computation. The amplitude normalization is given by  $\max |iT_{l'}| = 1$  at the surface.

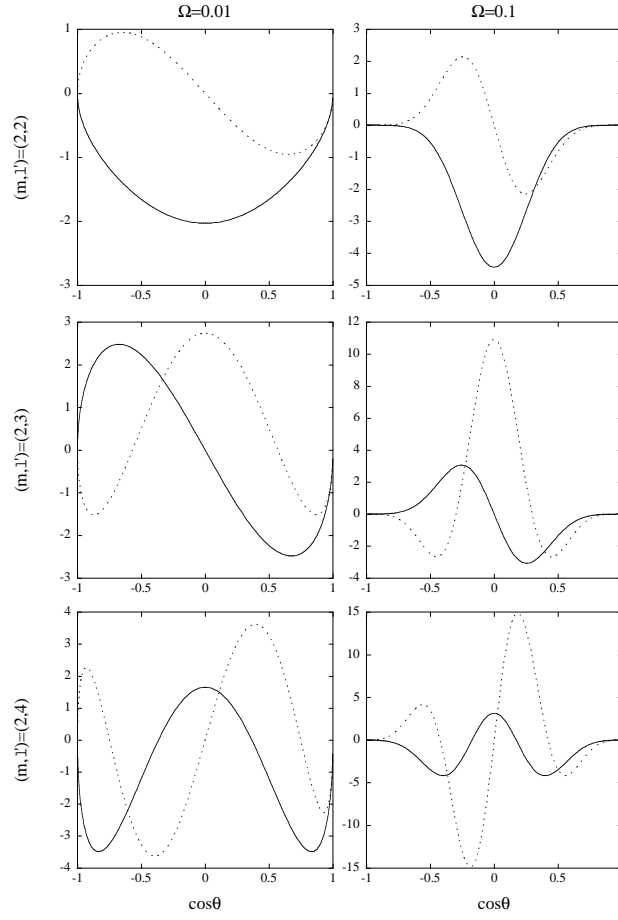


Fig. 10.— Same as Figure 9, but for  $m = 2$ .

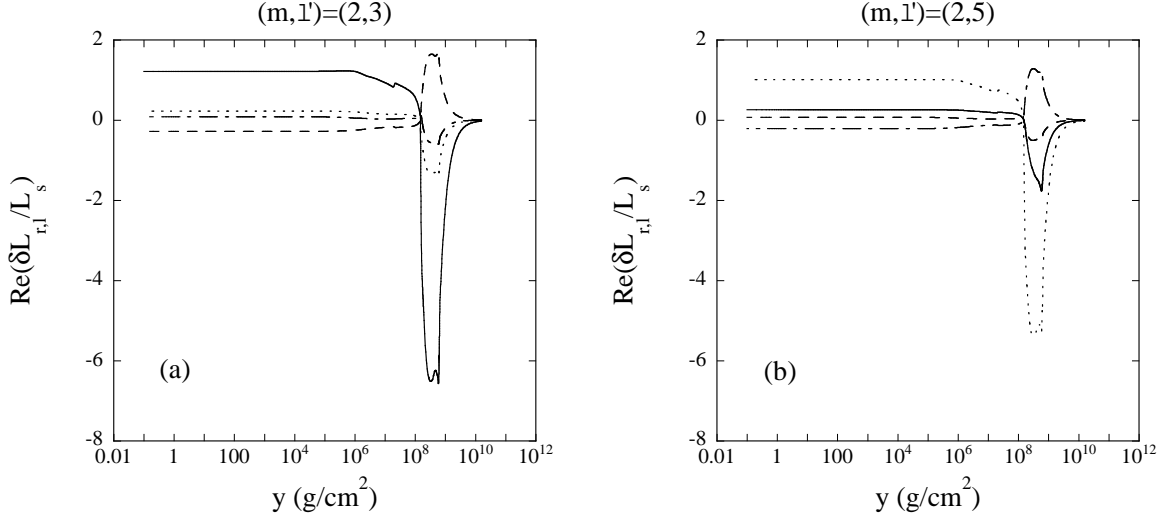


Fig. 11.— Expansion coefficients  $\Re(\delta L_{r,l}/L_s)$  of the fundamental  $r$ -modes at  $\bar{\Omega} = 0.1$  are given versus the column depth  $y$  for the convective model with  $\dot{M}/\dot{M}_{Edd} = 0.1$ , where the solid, dotted, dashed, and dash-dotted lines are for the coefficients associated with  $l = |m|$ ,  $|m| + 2$ ,  $|m| + 4$ , and  $|m| + 6$ , respectively. Panel (a) is for the  $r$ -mode of  $(m, l') = (2, 3)$ , and panel (b) is for the  $r$ -mode of  $(m, l') = (2, 5)$ . The amplitude normalization is given by  $\max |iT_{l'}| = 1$  at the surface.

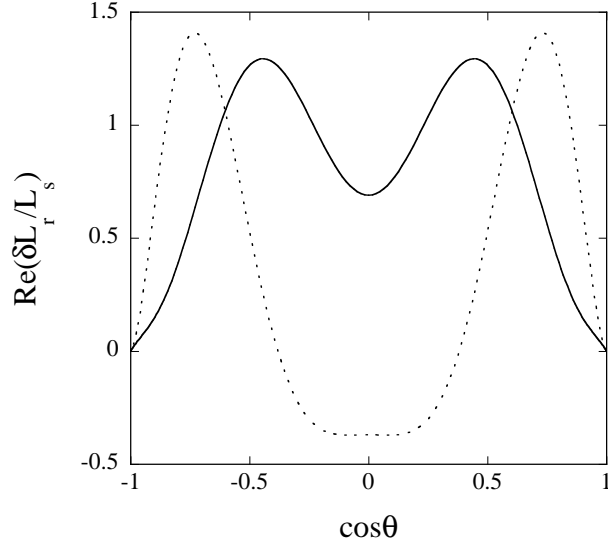


Fig. 12.—  $\Re(\delta L_r/L_s)$  at the surface is plotted as a function of  $\cos \theta$  for the fundamental  $r$ -modes of  $(m, l') = (2, 3)$  (solid line) and of  $(m, l') = (2, 5)$  (dotted line) at  $\bar{\Omega} = 0.1$  for the convective model with  $\dot{M}/\dot{M}_{Edd} = 0.1$ . The amplitude normalization is given by  $\max |iT_{l'}| = 1$  at the surface.